ELSEVIER

Contents lists available at ScienceDirect

# Ceramics International

journal homepage: www.elsevier.com/locate/ceramint



#### Review article

# Microstructure and mechanical properties of Ti–C–TiN-reinforced Ni204-based laser-cladding composite coating

Yu Zhao <sup>a,b</sup>, Tianqi Zhang <sup>a,b</sup>, Liaoyuan Chen <sup>a,b</sup>, Tianbiao Yu <sup>a,b,\*</sup>, Jiayu Sun <sup>c</sup>, Chuang Guan <sup>a,b</sup>

- a School of Mechanical Engineering and Automation, Northeastern University, Shenyang, 110819, China
- b Liaoning Provincial Key Laboratory of High-end Equipment Intelligent Design and Manufacturing Technology, Northeastern University, Shenyang, 110819, China
- <sup>c</sup> Deformation Processing Institute for Materials Research, Tohoku University, Sendai, 980-8577, Japan

#### ARTICLE INFO

Keywords: Ti/C/TiN Ni204 alloy Laser cladding Microstructure characteristics Mechanical properties

## ABSTRACT

In situ Ti(C, N), ring phase, and multi-phase enhanced Ni204-based alloy coating were prepared by adding various Ti/C/TiN ratios particles. The effects of the reinforcement phase on the microstructure, microhardness, tribological property, and microstructure characteristics at the interface between the coating and substrate were investigated. The results show that the coatings with a 5:1 mass fraction ratio of TiN/C exhibits the highest microhardness, which is 3.78 times higher than that of the original Ni204 coating. While, the coating with 21:7:2 mass fraction ratio of TiN/Ti/C exhibits the lowest friction coefficient, which is 4.44 times smaller than that of the original Ni204 coating. The addition of Ti and C particles promotes the precipitation of ring phase and carbides, reduces ceramic agglomeration, alleviates the floating of ceramic particles, and improves the bonding strength of reinforcement phases. Owing to the good mutual solubility among Fe, Ni, and, Cr elements, the diffusion happened at the interface between the coating and substrate.

#### 1. Introduction

The developing manufacturing industry has come an increased number of demands on the component, and a variety of issues keep on coming: poor wear resistance, corrosion, and lower hardness and service life [1,2]. The face-to-face or line contact components usually produce fracture, pitting, and bonding due to poor surface property. Reduce the service life and working stability of components. Therefore, enhancing the surface performance of components is an effective way to improve the service life. For steel parts, the surface properties obtained by post-treatment methods such as aging, quenching and tempering are difficult to meet all applications. There is an increasing solution in dealing with the waste components using remanufacturing technology, such as pitting, brush plating, surfacing [3,4], cold spraying [5], powder metallurgy [6], direct laser fabrication.

Considering the metallurgical bonding strength, porosity and cracks between substrate and coating interface, laser direct cladding composite materials is an effective method to improve surface properties. Using the direct Laser fabrication technology can improve the metallurgical bonding strength between the coating and the substrate [7–9], and the composite materials can solve the contradiction between coating

property and substrate bonding quality. To improve the performance of reinforced coating, wide attentions have been paid to composite metal material for which enhanced based alloy via adding or in situ synthesis reinforced phases. Liang et al. [6] built various contents of TiN and TiC composite coating via powder metallurgy technology. The addition of too much TiN to the coating would result in a reduction of wear resistance and compactness and an increase of porosity. Zhang et al. [10] used reactive hot pressing to fabricate a relative density, high hardness (1901 HV), and toughness (6.71 MPa m<sup>1/2</sup>) Ti(C, N)-TiB<sub>2</sub>-Co ceramics coating under sintered pressure at 34 MPa. Dobrzanski and Admiak [11] prepared ceramic/metal composite coatings by physical vapor deposition and investigated the reinforcement of TiN and Ti(C, N) on the high-speed steel. The difference in the substrate and coating was the failure mechanism. In YOU et al. [12] study, the TiN film was built on a ceramic surface via chemical vapor deposition. Ceramic powders have many excellent advantages, for example, high melting point, high hardness, high wear, and corrosion resistance, and good chemical stability. Addition a suitable content of ceramic powder is an effective method to enhance the properties of the metal-based material. Although the utilizing of the above methods can prepare the ceramic composite coating, the poor metallurgical bonding quality is still the critical factor

<sup>\*</sup> Corresponding author. School of Mechanical Engineering and Automation, Northeastern University, Shenyang, 110819, China. E-mail addresses: zhaoyuneu@gmail.com (Y. Zhao), tqz0120@126.com (T. Zhang), liaoyuanchen1024.neu@gmail.com (L. Chen), tianbiaoyudyx@gmail.com (T. Yu), sunjiayudewo@gmail.com (J. Sun), guanchuang10193@163.com (C. Guan).

affecting the coating properties [13–15]. The direct laser fabrication technology can fabricate an excellent density structure with good bonding quality, less internal defects, and high mechanical performance [16–18]. Therefore, many scholars have paid attention to the preparation of metal-based ceramic composites by direct laser fabrication.

The Ni-based powder is one of the most widely used self-melting alloy powder with corrosion resistance, oxidation resistance, good impact toughness, low melting point, and wide range of solid-liquid temperature [19]. Besides, the Ni-based alloy also has a strong wetting ability for a variety of matrix and WC particles. Not all Ni-based alloys can bond well with 45 steel easily, the properties some time have to be willing to compromise. Otherwise, the pores and cracks are easily generated in the interface zone. Ceramic-composite materials can be used to solve these issues, the number and type of in situ enhancement phase play a critical role in determining the coating properties such as microhardness and wear resistance. Saravanan et al. [20] investigated the effect of TiN on the wear behavior of SS 316 L. The hardness of TiN doped coating increased 9 times. The adhesion between the contact materials was prevented by the excellent bonding quality in TiN and matrix and the high hardness of TiN, thereby improving the wear resistance of the composite coating. Chen et al. [21] investigated the reinforcement of in situ synthesize Ti(C, N) and the small existing CeO<sub>2</sub> nanoparticles on Ni60 alloy. The microhardness and wear resistance of Ni60-based ceramic coating had changed with the addition of various ceramics. Zhao et al. [19,22] prepared Ni-based composite coatings with various mass fraction ratios of TiC/TiN/B<sub>4</sub>C via laser cladding. Although the hardness and wear resistance were significantly improved, the distribution of the ceramic phases was unevenly, thus caused big fluctuations of the mechanical properties. The density composite coating with better metallurgical bonding quality can be built utilizing laser cladding, while maybe the poor liquidity of ceramic powder and the breeding of cracks and pores causes the few studies using laser cladding. In the previous studies, Fe313/ceramic [15] and Ni204/ceramic [19,22] coating have been successfully built via laser cladding. The addition of existing ceramic caused relatively serious aggregation phenomena and the reinforcement of in situ synthesis ceramic phases is more stable. Microstructure characteristics, phases composition, and distribution of reinforcement phase direct effect the coating performance. There has seldom reported about in situ or exist ceramic reinforced Ni-based coating. The effect of ceramic content on the microstructure and mechanical properties is still an issue to be solved.

The reports of TiN, TiC, and Ti(C, N) reinforced Ni-based alloy via laser cladding are seldom. In this study, the composite coatings with various Ti/C/TiN/Ni204 mass fraction ratios were built on the 45 steel. The wear and hardness test were conducted and investigated the effect of ceramic content and characteristics on its mechanical properties. Further, the microstructure evolution mechanism and the microstructure characteristic in the interface between coating and substrate were also analyzed.

# 2. Materials and experimental procedures

The 45 stainless steel was used as the substrate and Ni204 alloy powder was chosen as the cladding material in this study, whose chemical composition is given in Table 1. The various mass fraction ratios of Ti/C/TiN was added into Ni204 alloy powder for investigating the reinforcement of ceramic phase, the specific proportion is shown in Table 2. Among them, the size of the sphere Ni204-based alloy powders ranges from 53 to 150  $\mu m$ , which provided by RAYCHAM Co. LTD. The

size of the sphere Ti particles (99.5% purity) is 53 µm, the size of the irregular graphite (99.95% purity) and TiN (99.5% purity) particles range from 0 to 53 µm and 2–10 µm, respectively. Ti, graphite, and TiN particles provided by Aladdin. These powders are averagely mixed as direct laser fabrication material. The milling time and speed have a significant effect on the powder's particle configuration. Choosing the tool small milling time and speed results in the powders being mix is not well, and the milling time and speed too large renders the mix powder failure because the powder size decreased, the more difficult deliver it becomes. Therefore, set the rotation speed = 30 rpm and mixed duration set up to 2 h. The ceramic ball to powder ratio ranges from 1.5 to 2 when mixing. Before and after mixing, the powders need to be dried under  $120\,^{\circ}\text{C}$  for 4 h.

The laser cladding experiments were conducted in an open-loop control system consisting of a 500 W YLR-500 optical fiber laser, water cooler, powder feeder, and a KUKA robot, the detail introduction has been reported in literature [16]. The offline software RobotArt was used to design cladding paths, the design and optimization of the cladding strategies have been discussed in detail in literatures [17,18]. The optimized argon gas flowing rate contributes to guarantee coating quality, so, the flowing rate of powder carrier gas (coaxially) is 8 L•min<sup>-1</sup> and the shielding gas (coaxially) is 15 L•min<sup>-1</sup>, which have been discussed in the literature [19]. The laser cladding parameters are given in Table 2 [19,22].

To use a wire-electrode cutting machine to prepare all specimens, the specimen surface was ground, polished, cleaned, and dried. The metallographic specimens were etched in a 2:1:1 vol HCl: HNO<sub>3</sub>: H<sub>2</sub>O hybrid solution. X-ray diffraction (XRD) was used to identify the phase constitutions, the diffraction angle ranges from  $5^{\circ}$  to  $90^{\circ}$  with a scanning speed of  $12^{\circ}$ -min<sup>-1</sup>. The wear morphology of the specimen surface was characterized by laser confocal microscopy (OLYMPUS LEXTOLS4100). The microstructure in the cross-section of the coating and the interface of the substrate-coating was observed by a field emission scanning electron microscope (SEM, Zeiss Ultra Plus) which equips with the electron backscatter diffraction (ESBD) and Energy dispersive spectrometer (EDS). The microhardness tester (EM500-2 A) and reciprocating friction wear tester (MFT-4000) were used to investigate the reinforcement of in situ TiN, TiC, Ti(C, N), and other carbides. The other detailed experiment parameter of needs can be got from Refs. [19,22].

## 3. Results

#### 3.1. Coating phase analysis

Fig. 1 shows the XRD pattern of all specimens. The diffraction peaks of TiC, TiN, and Ti(C, N) were detected in specimens 2#-5#. However, no TiC and Ti(C, N) peaks are found in specimen 1#. In 30% TiN/70% Ni204-based composite coating (specimen 1#), aside from TiN, the (Fe, Ni) solid solution, (Fe, Cr) solid solution, and Ni–Cr–Fe were also detected. And, more remarkable, the separate peak for each diffraction. With the addition of C particle (specimen 5#), the characteristic of the diffraction peaks changed. There appears to be more than one peak in diffraction near TiN peak, the TiC and Ti(C, N) phases were in situ formed. When various mass fraction ratios of Ti/C/TiN particles were added to Ni204, the characteristic of diffraction peak around TiN is continually changing (specimens 2#-4#), the MC<sub>X</sub> (M = Fe, Nb, Cr, Mo) precipitation increases and the intensity of peak decreases.

The following reactions occurred between Ti, C, N, and other metal elements caused these changing:

Table 1 Chemical composition of Ni204 powder and #45 die steel (wt. %).

	С	P,S	Si	Cr	Ni	Mn	Mo	Nb	Cu	Fe
Ni204	≤0.03	_	0.4	21	Bal.	_	9	4	_	1.5
45 steel	0.42 - 0.5	≤0.045	0.17-0.37	≤0.25	≤0.25	0.5-0.8	-	_	≤0.25	Bal.

Table 2
Composite of cladding materials and laser cladding parameters (wt. %).

No.	Compon	ent con	tent (w	vt %)	Process parameters				
	Ni204	Ti	С	TiN	Laser powers (W)	Scan speed (mm•s <sup>-1</sup> )	Powder feeding rate (r•min <sup>-1</sup> )	overlap rate (%)	Δz (mm)
1#	70	0	0	30	450	5.5	0.7 (11.056 g•min <sup>-1</sup> for Ni204-based alloy powder)	35	0.35
2#	70	12	8	10					
3#	70	12	3	15					
4#	70	7	2	21					
5#	70	0	5	25					

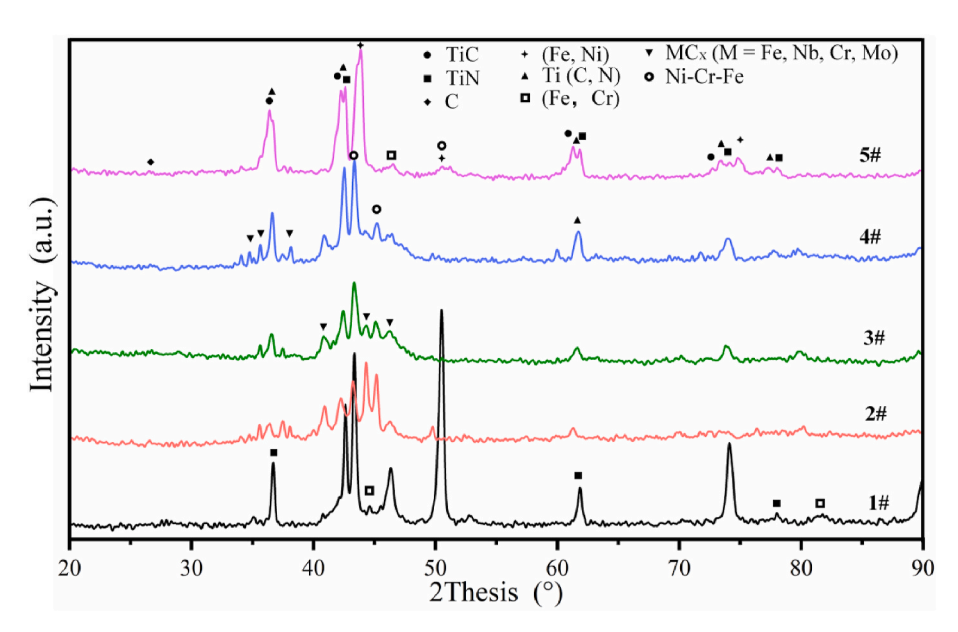


Fig. 1. XRD patterns of coatings with various Ti/C/TiN ratios.

$$Ti + C \rightarrow TiC (1)$$

$$xTiC + yTiN \rightarrow Ti(C_x, N_y) (0 < x, y < 1, x + y = 1) (2)$$

$$M + xC \rightarrow MC_X (0 < x < 1, M = Fe, Cr. Mo, and Nb) (3)$$

Ti can combine with C to form TiC, the relationship between temperature and Gibbs free energy of formula (1) is an approximately linear function  $\Delta G_T^\theta = -184.096 + 0.012099 T (kJ \, mol^{-1}) \,$  [23]. The Gibbs free energy of formula (1) was -158.7 kJ  $mol^{-1}$  at 2100 K, and the  $\Delta G_T^\theta < 0$  when the temperature ranges from 298 K to 2100 K, indicating formula (1) can be spontaneous during laser cladding. TiC and TiN have a similar lattice structure, so they can easily precipitate and aggregate to form Ti (C, N) ternary phase. The Gibbs free energy of the formation of Ti(C, N) (formula (2)) can be calculated by Ref. [24–26],

$$\Delta G_T^{\theta} \left[ TiC_x TiN_y \right] = x \Delta G_T^{\theta} \left[ TiC_x \right] + y \Delta G_T^{\theta} \left[ TiN_y \right] + RT \left\{ x lnx + y lny \right\}$$
 (4)

where R stands for the general gas constant (R = 8.314 kJ<sup>-1</sup>), Ti(C<sub>0.2</sub>, N<sub>0.8</sub>), Ti(C<sub>0.3</sub>, N<sub>0.7</sub>), and Ti(C<sub>0.7</sub>, N<sub>0.3</sub>) are the most common forms of Ti (C<sub>x</sub>, N<sub>y</sub>) phases. In the literature [24], the Ti(C<sub>0.2</sub>, N<sub>0.8</sub>) was considered as the thermodynamically favorable phase. The Gibbs free energy of formulas (1) and (2) is negative under the cladding temperature, the absolute value of  $\Delta G_T^{\theta}$  [formula (2)] >  $\Delta G_T^{\theta}$  [formula (1)], this is leading to be better to the formation of Ti(C<sub>0.2</sub>, N<sub>0.8</sub>).

Due to the addition of C particles, the high Cr content of Ni204 alloy has contributed to the formation of  $CrC_x$ . In general, x is 3/2, 3/7, and 6/23, the expression of various  $CrC_x$  Gibbs free energy are given [23]:

$$Cr_2Cr_3: \Delta G_T^{\theta} = -85.35 - 0.020727T(kJ/mol)$$
 (5)

$$Cr_6Cr_3: \Delta G_T^{\theta} = -161.92 + 0.017357T(kJ/mol)$$
 (6)

 $Cr_{23}C_6$ :  $\Delta G_T^{\theta} = -364.84 + 0.029154T(kJ/mol)$  (7).

From the value of  $|\Delta G_T^\theta|$ , precipitation stability and order of  $Cr_{23}C_6$ ,  $Cr_6C_3$ , and  $Cr_2C_3$  successively reduced. The Fe can replace Cr in  $CrC_x$  to form (Cr, Fe)  $C_x$ . The matrix has higher concentrations of C when added C, the C combined with M (M = Fe, Cr, Nb, Mo, and Ti) to form  $MC_x$ . It was confirmed that formulas (1)–(3) can be spontaneous.

# 3.2. Coating composition and microstructure analysis

The elements mapping distribution of the square-shaped phase in specimen 2# was detected, as shown in Fig. 2. One can find that the square-shaped phase is core-shell structure, and Ti, N, Nb, and Mo were detected in this structure, maybe some C atoms exist in it [19]. As the results in Fig. 2(b)-(e), Ti and N are mainly distributed in the core zone and the shell zone primarily contains Nb and Mo. Based on the feature of laser cladding, the smaller size of TiN can decompose into Ti and N while a larger one leads to complete decompose failure, and only partially or not. Ti and C gathered around the undecomposed TiN particles to form Ti(C, N) and TiC owing to the similar crystal structure. Besides, Nb is also attracted to the C atoms to form NbC. Mo has an important role in preventing the development of carbides [27], so Mo would gather around carbide phases (TiC), forming (Nb, Mo, Ti) (C, N) multi-ring phase. The results gained by energy spectrum analysis (ESP) of points 1 and 2 are given in Table 3. In point 1, the phase is TiN. while in point 2, the content of Ti and N decreased, Nb and Mo present the reverse. Combine with Fig. 2 and previous research [19,22], the phase at point 2 area was determined as (Nb, Mo, Ti) (C, N).

The line distribution of Ti, N, C, Nb, Mo, Ni, Fe, and Cr from the

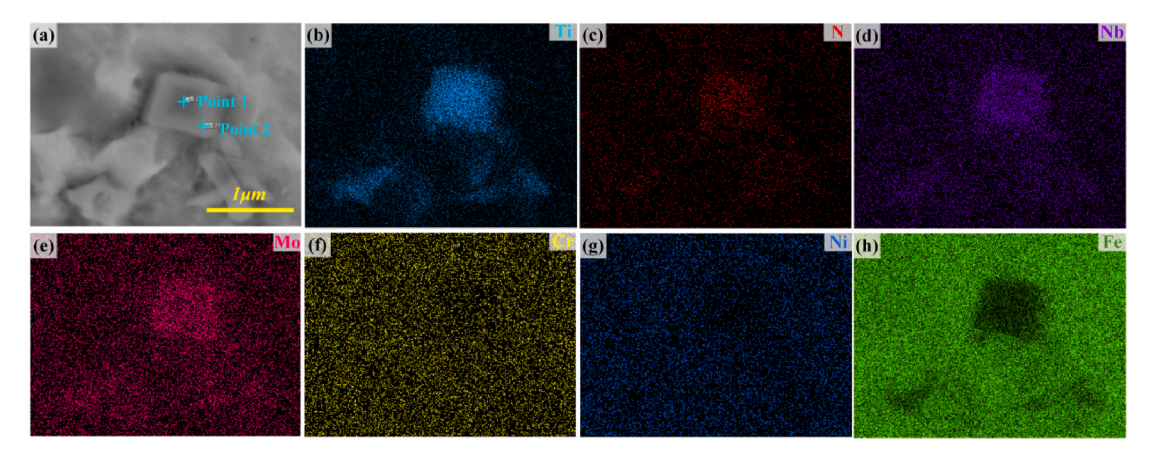


Fig. 2. EDS maps showing the distribution of Ti, N, Nb, Mo, Fe, Cr, Ni, and Fe in sample 2#.

Table 3 EDS spectra analyses results of samples (au. %).

Marked locations	Ti	C	N	Nb	Mo	Ni	Cr	Fe	Si
Point 1	50.41		10.82	4.33	1.60	1.20	1.08	30.57	
Point 2	35.18			5.38	2.90	2.24	1.59	52.15	0.57
Point 3	3.01			1.66	4.69	38.81	15.61	35.27	0.95
Point 4	1.25			1.12	2.38	23.80	9.67	61.03	0.74
Point 5						0.01		98.49	0.66
Point 6								98.67	0.49
Point 7	3.73					4.86	2.00	89.40	
Point 8	1.35				0.37	5.56	2.35	90.37	
Point 9	38.19			4.89	1.76	2.33	1.65	51.18	
Point 10				6.56	24.15	18.36	22.02	28.01	0.9
Point 11	53.65		46.35						
Point 12	3.8				2.31	37.47	13.67	42.07	0.69
Point 13	23.17			2.01	6.30	28.48	19.38	20.66	
Point 14	78.66		21.34						
Point 15	19.72			3.24	6.35	27.69	10.44	32.57	
Point 16	23.49			0.63	2.48	28.14	11.23	34.03	
Point 17		100							
Point 18	52.96		47.04						
Point 19	55.66		44.34						
Point 20	1.25			0.37	2.68	39.53	15.54	40.64	
Point 21	3.77			2.76	5.98	38.61	16.26	32.61	
Point 22	24.15			25.31	9.46	15.12	9.76	16.20	
Point 23	5.45			5.66	5.09	36	14.55	33.25	

substrate to coating is presented in Fig. 3. Four areas, substrate, heataffected zone (HAZ), coating 1, and coating 2, appeared in the coating. According to the results, the distribution of Nb and Mo in the whole coating is uniform. The diffusion of Ni, Cr, Fe, and C happened in the interface between the substrate and coating and the interface between the coating 1 area and coating 2 area. When the substrate was irradiated by the laser, the Ti/C/TiN-Ni204 composite powder associated with the melted substrate as the coating 1 area. Also note that the Ti, C, and TiN floated up during laser cladding, which kept consistent in literatures [19,22]. At the interface between coating 1 and coating 2, the content of Cr, Ni, and Fe is not a sudden change. The different concentrations in these areas caused diffusion. Fe can dissolve in Ni liquid phase without limit to form [Fe, Ni] solid solution, therefore, the content of Fe is gradually decreased in the coating 2 area. Test the points 3–6 by ESP, the results are given in Table 3. The 98.49% and 98.67% Fe was detected in point 5 (HAZ) and point 6 (substrate), respectively. The microstructure of the HAZ has been refined due to the laser radiation. The 61.03% Fe, 1.25% Ti, 1.12% Nb, 2.38% Mo, 23.8% Ni and 9.67% Cr were detected in point 4 (coating 1 area). In the coating 2 area, 35.27% Fe, 3.01% Ti, 1.66% Nb, 4.69% Mo, 38.81% Ni, and 15.61% Cr were detected in point 3, these results were same with the line scanning.

The cross-section morphology and microstructure of the substrate, the HAZ, and coating under various mass fraction ratios of Ti/C/TiN/

Ni204 are shown in Fig. 4. Fig. 4(a)–(e) indicate that there is an obvious interface among substrate, HAZ, and coating. The good metallurgical bonding in substrate and coating was formed, no pores and cracks appeared around this area. While some cracks appeared in the coating of specimens 2#-4#. On the one hand, the cracks may be caused by remelting during laser processing, and on the other hand, the difference in thermal expansion coefficients between ceramic particles and the matrix which induced thermal stress, providing the source to crackle. The TiC particles would rise towards the surface direction and its characteristics have a direct relationship with fusion temperature. The edge angle and irregular shape of TiC particles weaken as temperatures go up [28]. At the top of each layer, the concentration of TiC is higher, and the size is bigger. According to the analysis of cladding temperature distribution in the literature [16], the temperature of the overlapping zone generated by adjacent layers is lower than other zones, therefore, the size of the ceramic particles at this zone is bigger, causing an obvious layered structure, as shown in Fig. 4(b)-(d). Specimens 1# and 5# are added 30% TiN and 25% TiN-5% C, respectively. So, there is no layered structure. Fig. 4(a1)-(e1) show the SEM images of the substrate and no change in microstructure. Fig. 4(a2)-(e2) are the microstructure of the HAZ. Although there is no change in the contents of elements, the microstructure characteristics are quite different from the substrate zone. Under the influence of laser radiation, the milk-white ferrite and

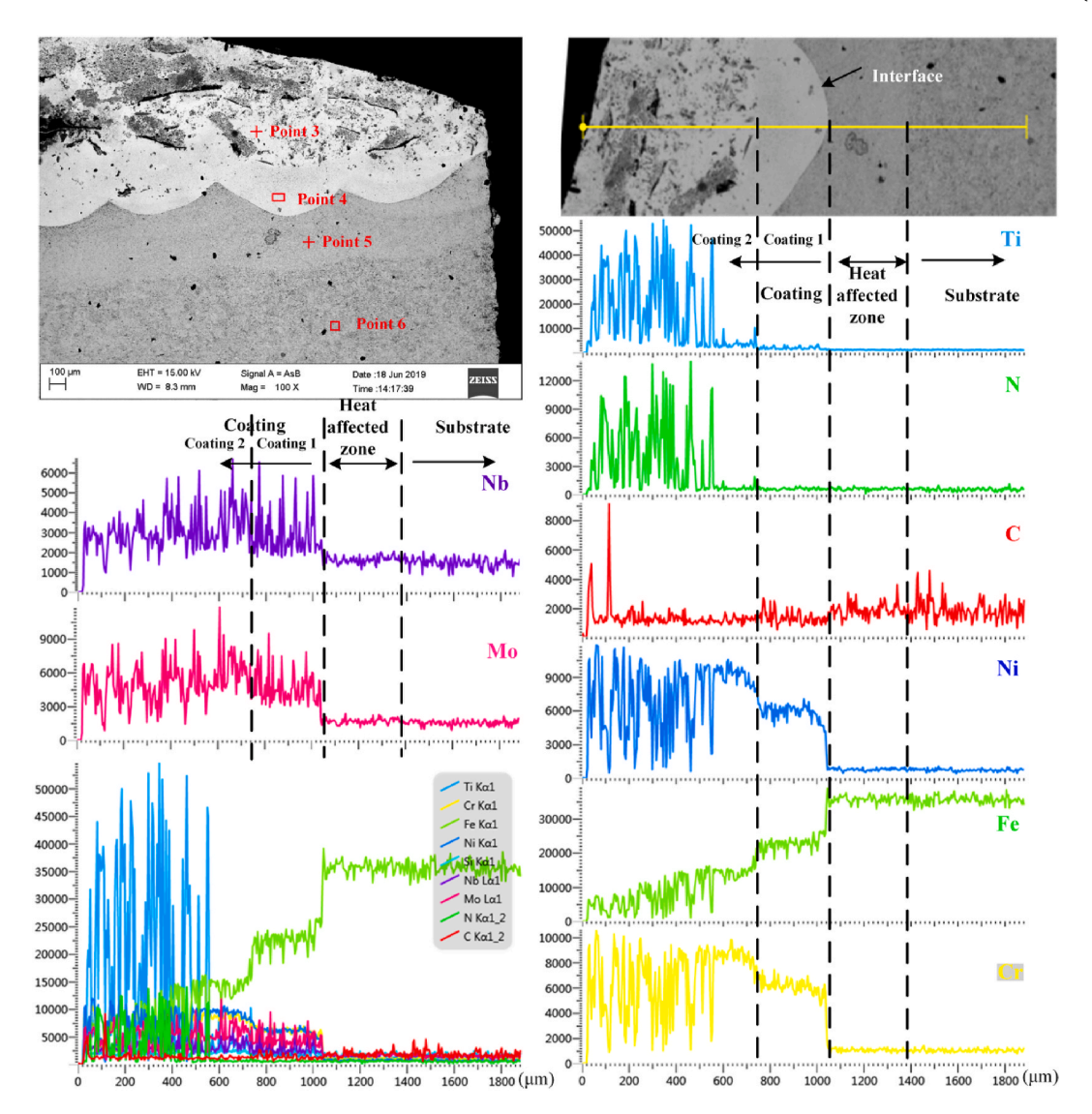


Fig. 3. EDS line scan results of Ti, N, C, Nb, Mo, Fe, Cr, and Ni in sample 1#.

calls lamellar pearlite disappeared (Fig. 4(a2)), and the grain of the HAZ was refined (Fig. 4(e2)). Besides, the soon hot and cold feature makes the recrystallization austenite grains failed to grow up, changing the state of the original coarse grains. Owing to the multiple remelting and heat treatment that happened at the HAZ, many nanocrystalline generated, as shown in Fig. 4(b2)–(d2).

The microstructure characteristics of the bottom of the coatings (coating 1 area) were observed (Fig. 4(a3)–(e3)). When the 30% TiN was added in specimen 1#, the microstructure characteristic is similar to pure Ni204 alloy. According to the previous study, the milk-white phase is a secondary precipitate phase [Nb, Mo]. The size of the addition TiN is 2-10 µm, TiN particles are easy-melted and trended to float up, thus there is seldom TiN particles appeared in this zone (Fig. 4(a3)). The TiN/ Ti/C mass fraction ratios of specimens 2#-4# are 5:6:4, 5:4:1, and 21:7:2, respectively. The number of block-shape ceramic phase increases as the TiN content increases. From Fig. 4(c3), one can find that the reinforcement phase precipitated firstly at the grain boundaries. The Ti, N, and C elements dissolved into Ni-based alloy liquid to form Ti-N-C-Nb-Mo-Cr-Fe-Ni multivariate liquid phase, and then TiC, TiN, Ti(C, N) and other carbides were precipitated. The size of Ti particles is 100 µm, when Ti and C particles were added into Ni204 alloy, increased the appearance of Ti(C, N) and carbides at the bottom of the coating, thus alleviated the floating of ceramic particles (Fig. 4(b3) and (c3)). In

order to analyze the phase composition, points 7 and 8 were detected by ESP, the results are given in Table 3. The 89.4% Fe, 3.73% Ti, 4.86% Ni, and 2% Cr were detected in the white phase (point 7). Owing to 8% C particles were added into the coating and the untrusted data of C content by ESP, combined with Table 2 and Fig. 1 (XRD results), the phase is FeC<sub>x</sub>. At point 8, 90.37% Fe, 1.35% Ti, 5.56% Ni, and 2.35% Cr, the matrix is Fe rich solid solution, which indicates the diffusion occurred at molten pool boundary, and the results agree with Fig. 3. From point 9, the phase is cell-shell structure, the cell area primarily contains 38.19% Ti, indicating this phase is TiC, the phase of shell area can be confirmed as ring phase (Ti, Mo, Nb)C [19,22].

Fig. 5 show the SEM images of the specimens with various Ti/C/TiN mass fraction ratios and the ESP measured results are presented in Table 3. When only added 30% TiN into the Ni204 alloy, many bigger and irregular ceramic phases appeared in the coating 2 area. The incomplete melting TiN particles aggregated together to form the large TiN phase, as shown in Fig. 5(a). The white phase in specimen 1# (point 10) which is near the gray phase primarily contains 6.56% Nb and 24.15% Mo. The Nb, Mo, Ti, and N atoms dissolved into Fe–Ni–Cr liquid phase, the TiN precipitated firstly at the grain boundary and in the intergranular, and then the Nb and Mo precipitated at the grain boundary in the form of secondary precipitated phase (Nb, Mo). The 53.65% Ti and 46.35% N were detected in point 11 area, combined with

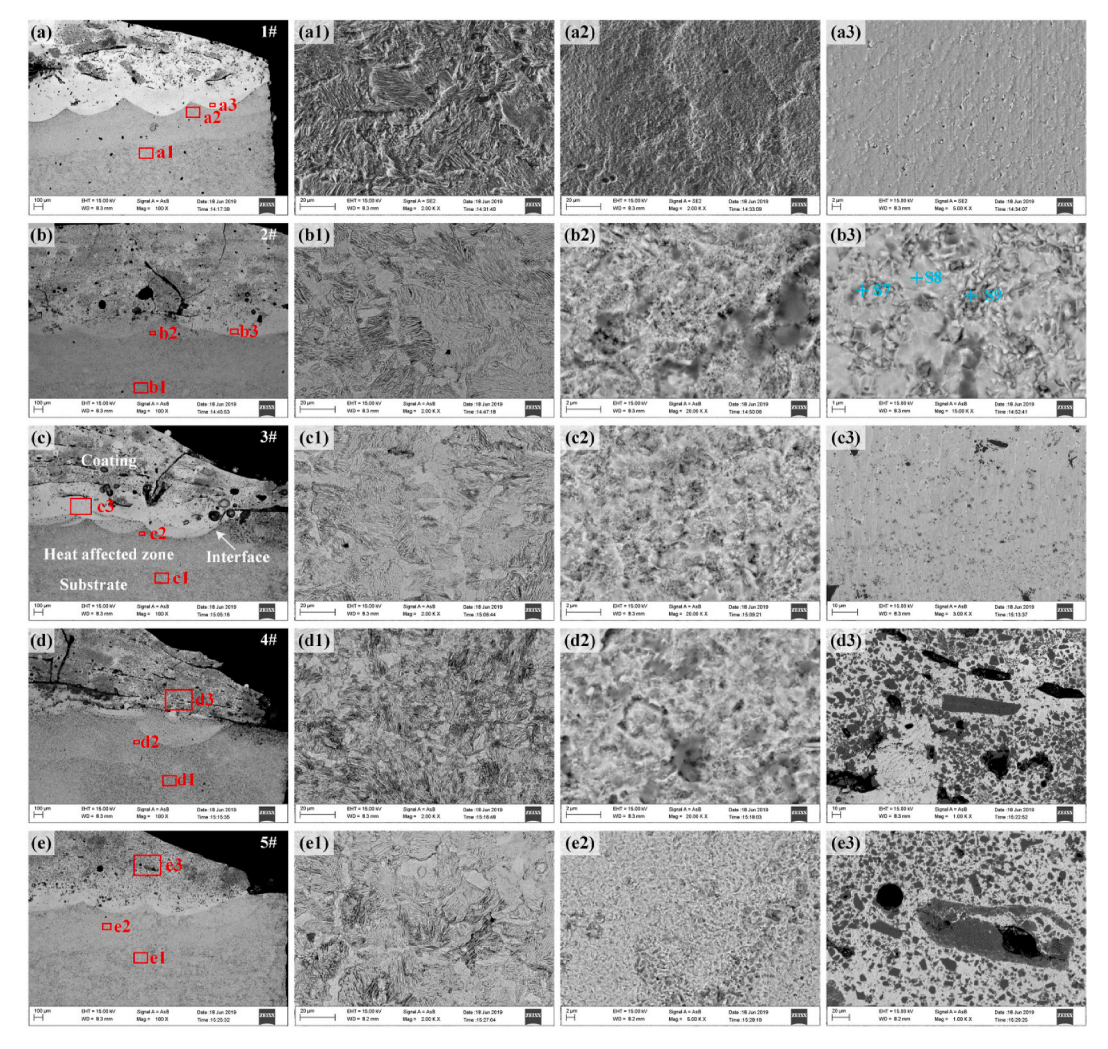


Fig. 4. Microstructure and morphology of samples. (a)–(e) Cross-section morphology; (a1)–(e1) Microstructure on the substrate; (a2)–(e2) Microstructure on the HAZ; (a3)–(e3) Microstructure on the coating.

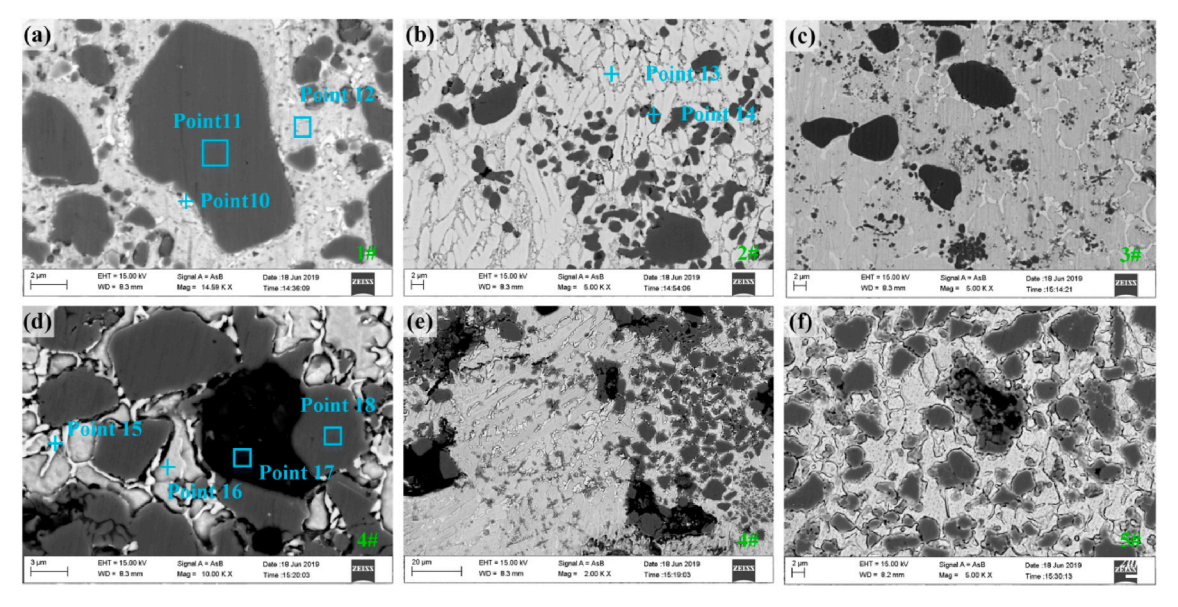


Fig. 5. BSE images of coatings. (a) Sample 1#; (b) Sample 2#; (c) Sample 3#; (d), (e) Sample 4#; (f) Sample 5#.

the XRD results obtained in Fig. 1, indicating the phase is TiN. In the matrix area (point 12), the 3.8% Ti, 2.31% Mo, 37.47% Ni, 13.67% Cr, and 42.07% Fe were detected, indicating the matrix mainly consists of Cr, Ni, and Fe element, some tiny TiN particles dissolved in it. When Ti, C, and TiN particles were added into Ni204 coating, the microstructure characteristics changed (Fig. 5(b)-(e)). With the content of TiN increases, the size of ceramic particles increased. From Fig. 5(b), the microstructure of this specimen mainly contains gray phase (arc boundary) and milk-white phase (columnar-shape), and the microstructure characteristic at the grain boundaries changed. The 23.17% Ti, 2.01% Nb, 6.3% Mo, 28.48% Ni, 19.38% Cr, and 20.66% Fe were detected in point 13, according to Fig. 1, the matrix phase can be determined as Ni-Fe-Cr, [Fe, Ni] and [Fe, Cr] solid solution. The tiny TiN, TiC particles, and other carbides dissolved into the matrix. In point 14, 78.66% Ti was detected, while just 21.34% N in this point, combined with Fig. 1 and the C addition content, the phase in this point is Ti(C, N). The high concentration of C has reduced the (Nb, Mo) precipitation. which in turn increases the MC<sub>x</sub> (M = Fe, Cr, Nb, Mo) content. With the decreases of C content, the size of the precipitated ceramic phase reduced, as shown in Fig. 5(c) and (e). The white long-chain phase appeared at the grain boundary, which is similar to Fig. 5(a). Fig. 5(d) is the enlarged SEM image of Fig. 5(e). The white long-chain phase (point 15) primarily contains 19.72% Ti, 3.24% Nb, 6.35% Mo, 27.69% Ni, 10.44% Cr, and 32.57% Fe. One can find that the concentration of Nb and Mo in point 16 is reduced, therefore, the long-chain phase can be determined as (Nb, Mo). The matrix mainly consists of Ni-Cr-Fe and [Fe, Ni] solid solution, and the in situ synthesis tiny TiC particles dissolved into the matrix; the 100% C was detected in point 17, indicating the black phase is graphite; the gray phase mainly contains 52.96% Ti and 47.04% N, the gray phase is TiN. The incomplete melting large TiN particles, C, and Ti attracted each other, the in situ formed TiC dispersed through the matrix and dissolved into TiN particles to form Ti(C, N), the C that failed reaction to form graphite. The graphite mainly appeared at the overlapping zone between adjacent layers.

The obvious cell-shell structure appeared in the specimen 5# which was added 25% TiN and 5% C (Fig. 5(f)). In the previous studies [19,22], the gray phases of cell areas are TiN, TiC, and Ti(C, N), the shell areas are multi-ring phase (Ti, Nb, Mo) (C, N). At the grain boundary, the precipitation phase also changed. The MCx (M = Fe, Cr, Nb, Mo, Ti) has replaced (Nb, Mo).

The phase composition in Fig. 6 (specimen 1#) can be acquired through ESP. The testing results of points  $19{\text -}23$  were presented in Table 3. The gray phase (point 19) contains 55.66% Ti and 44.34% C, combined with XRD results obtained from Fig. 1, indicating this phase is TiN. The 39.53% Ni, 15.54% Cr, and 40.64% Fe were the main detected elements in point 20. During laser cladding, the Mo, Nb, N, and Ti precipitated out in form of TiN and (Nb, Mo), so, the matrix consists mainly of Cr–Fe–Ni, [Fe, Ni] and [Fe, Cr] solid solution. Fig. 6(b) is the

enlarged SEM image of the grain boundary area. At points 22 and 23 area, 24.15% Ti, 25.31% Nb, 9.46% Mo and 5.66% Nb and 5.09% Mo were detected, respectively. Which can be confirmed as (Nb, Mo), meanwhile, some tiny TiN dissolved into it.

### 3.3. Microhardness of the composite coating

The microhardness distributions arrange from the substrate to the coating surface of the composite coatings with various Ti/C/TiN/Ni204 mass fraction ratios are measured and shown in Fig. 7. Owing to the in situ formation of TiC, Ti(C, N), TiN, and other carbides, meanwhile, the existence of dispersion strengthening and solution strengthening, the microhardness of the coating 5# is 3.78 times higher than that of Ni204based alloy coating (298 H V). The various Ti/C/TiN ratios enhancement on the Ni204 coating is in the following order: sample 5# > sample 4# > sample 2# > sample 1# > sample 3#. The specimens 2#-4#showed similar transformation trends, and specimen 1# is the same as specimen 5#. When Ti and C doped into Ni204/TiN composite coating, the ceramic particles floating have been weakened by the in situ synthesize Ti(C, N). The dispersion strengthening of TiC and carbides also enhanced the microhardness at the bottom of the coating. When 12% Ti, 3% C, and 15% TiN particles were added, the microhardness of the coating surface among all specimens is lowest. According to Fig. 5, the size and number of ceramic phases are less, and the floating up of TiN particles caused the relatively poor reinforcement. Owing to 8% C particles were added to the specimens 2#, although the TiN content decreased, the in situ synthesis TiC, Ti(C, N), and carbides increased. The TiC, Ti(C, N), and MC<sub>x</sub> (M = Cr, Fe, Mo, Nb) enhanced the microhardness. The coating 4# has the highest microhardness among specimens 2#-4#, which was profited from the addition of 7% Ti, 2% C, and 21% TiN, the high content of the reinforcement phase and good bonding strength between the reinforcement phase and the matrix. Compared with specimen 1#, the in situ synthesis TiC and Ti(C, N) phases in specimen 4# have effectively enhanced the coating. Therefore, the specimen presents a higher hardness. The specimen 5# was added 25% TiN and 5% C, the C play an important role in generating the multi-ring phase (Ti, Nb, Mo) (C, N) and multi-phase (Cr, Fe, Nb, Mo)C. The TiN and C were easy to in situ forms Ti(C, N), thus increasing the concentration of C around TiN. And then, the content of Nb increased and dissolved into Ti(C, N) to form (Ti, Nb) (C, N). Mo can prevent carbon from growing up, thus Mo spread to (Ti, Nb) (C, N) to form the multiring phase (Ti, Nb, Mo) (C, N). Owing to the addition of C, the Cr and Fe precipitated in the form of (Cr, Fe)C at the grain boundary, combined with the (Nb, Mo) phase to form (Cr, Fe, Nb, Mo) C. The multi-ring phase improved the bonding force between ceramic phase and matrix. Besides, the carbides precipitation at the grain boundaries also improved the intensity of intergranular.

When the force was applied on the surface, the micro-cracks

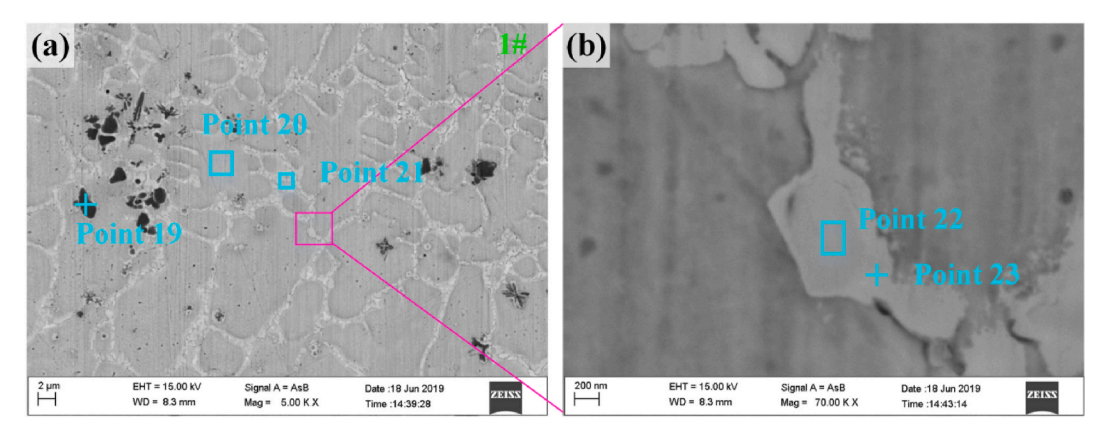


Fig. 6. Microstructure and spectrum analysis of sample 1#.

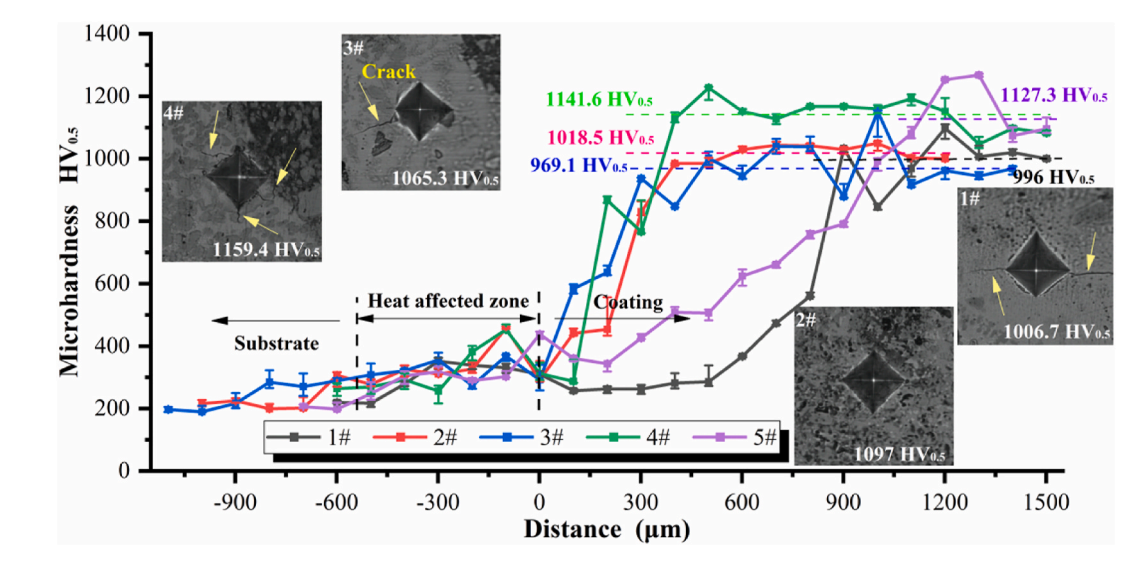


Fig. 7. Microhardness of different samples.

generated on the surface. With the microhardness increased, the crack branch and total crack length increased. All specimens appeared concentric ring cracks and the residual Vickers impression generated in specimen 4# was irregular lines [29]. Although the hardness of Ni204-based alloy coating was enhanced by adding various Ti/C/TiN ratios particles, the fracture toughness decreased.

#### 3.4. Friction coefficient of the composite coating

Friction coefficients change curves of the composite coatings with

different Ti/C/TiN/Ni204 mass fraction ratios over time are present in Fig. 8. According to the previous study [19,22], the abrasive wear and adhesive wear is the dominant wear dominant. Therefore, friction coefficient values increased in the initial stages (Fig. 8(a')), after several minutes of turmoil, the trend of the values to level off, oscillating up and down around a stable value (Fig. 8(b')). It was supposed that the increment in the coefficient friction value was owing to the grinding ball breaking the smooth surface. As the wear time goes on, the surface materials flaked off and accumulated, causing a shakeout stage for coefficient friction values, namely the run-in period. The content, kind,

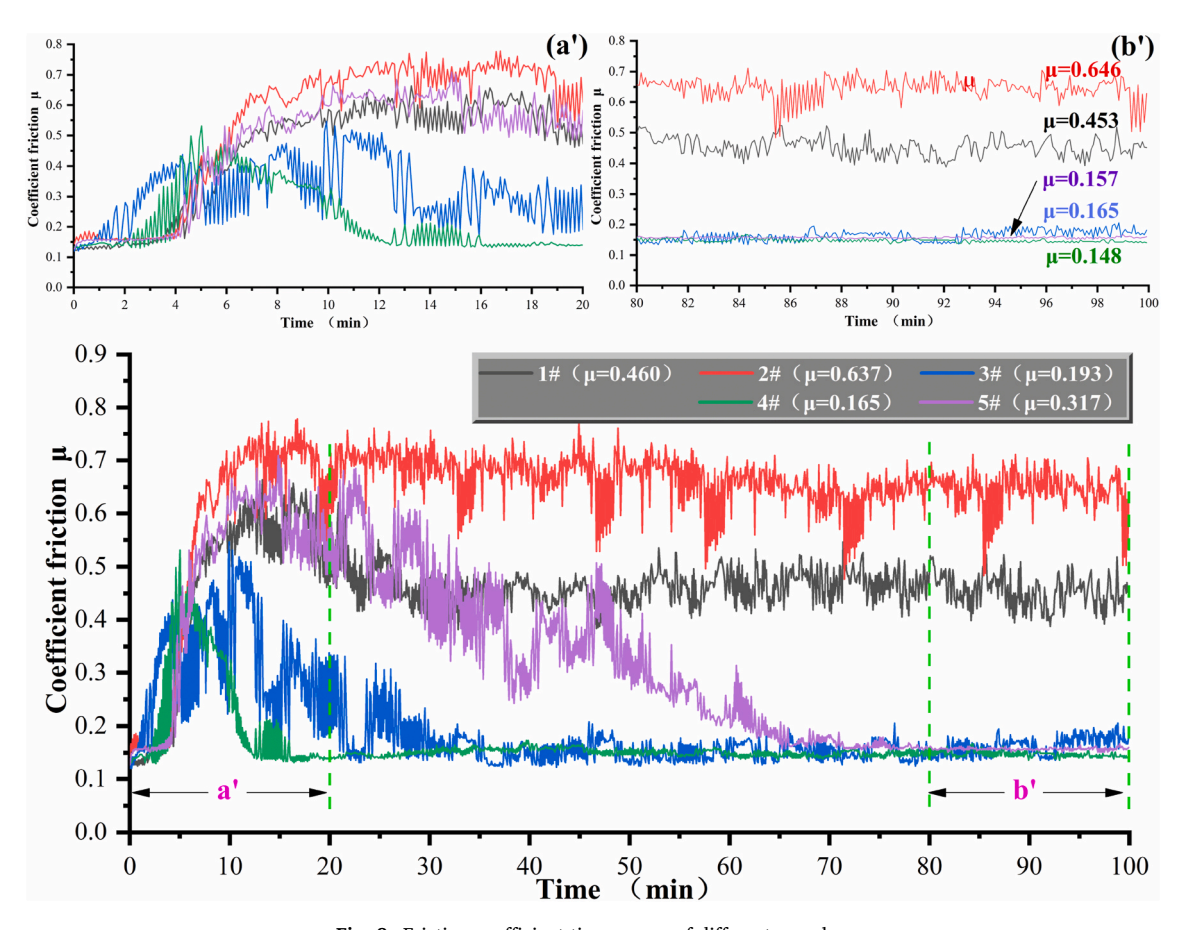


Fig. 8. Friction coefficient-time curves of different samples.

and size of peel off materials in the wear areas achieved a dynamic equilibrium and were responsible for the stable stage [30,31]. The friction behavior of the composite coatings changed with the content of Ti, C, and TiN particles, and the distribution, content, size, and characteristics of the reinforcement play an important role. Use the average coefficient friction value which ranges from 80 to 100 min as the coefficient friction of the specimens, the order of the coefficient friction follows by, sample 2# > sample 1# > sample 3# > sample 5# > sample4#. From Fig. 8(a'), one can find that the time for the specimens to reach stability is in order: sample 5# >sample 3# >sample 1# >sample 4# > sample 2#. Only TiN was added, the TiN easily appeared agglomerate, had a larger size, and generated poor bonding force with the matrix, thus needing more time to cause the TiN particles to peel off, and causing the disadvantageous effect of wear resistance. When TiN and C were added together, the in situ synthesize Ti(C, N), multi-ring phase (Ti, Nb, Mo) (C, N), and MC<sub>x</sub> (M = Cr, Fe, Nb, Mo) improved the bonding force between reinforcement and the matrix, and the bonding force in the intergranular. Therefore, more wear time was needed to peel off the reinforcement, and the reinforcement and carbides improved the wear resistance. When various contents of TiN, Ti, and C were added, the wear mechanism changes. With the addition content of TiN decreased, the wear resistance weakened. The size of the in situ formation reinforcement particles, such as TiC, MCx, was small, which was primarily a diffuse distributed in the coating. These particles were easily peeled off and had a disadvantage for the improvement of wear resistance. As the same bonding strengthening, the reinforcement size and content is important for the wear resistance. The 21% TiN, 7% Ti, and 2% C particles were added into specimen 4# was added the Ti and C particles improved the bonding strength between the reinforcement phases and matrix, and also guaranteed the content and size of reinforcement. Thus, specimen 4# showed lower friction coefficient values.

The two-dimensional and three-dimensional morphologies of scratches of the specimens with various Ti/C/TiN/Ni204 mass fraction ratios are given in Fig. 9. The adhesive phenomenon appeared on the wear areas of specimens 1# and 5# (Fig. 9(a) and (e)). In specimen 1#, the matrix was enhanced by TiN while the composite of the phases remained unchanged. So in the wear stage, the soft matrix was easily peeled off and appeared adhesive wear. The large volume TiN particles improved the ability to resist the deformation. Therefore, the friction coefficient is a factor 1.45 smaller than that of the initial coating. (friction coefficient of Ni204 is 0.657). From Fig. 5(f), one can find that the large content of carbides was generated in the coating. On the one hand, the bonding strengthens between the reinforcement phase (TiN, TiC, and Ti(C, N)) and matrix was enhanced, improving the wear resistance, and on the other hand, the content of carbides (MCx) in the peel-off materials improved, causing the adhesive of the wear surface (Fig. 9(e)). In specimens 2#-4#, the in situ formation TiC and Ti(C, N) uniform distributed in the coating. However, sample 2# was added 8% content of C which caused low lump ceramic phases density. Aside from in situ synthesis TiC, there were also many carbides (MC<sub>v</sub>, M = Fe, Cr, Nb, and Mo). The hardness and wear resistance of the carbides are all poor to TiN, TiC, and Ti(C, N) ceramic particles, so wear resistance is the worst. From the wear surface (Fig. 9(b)), the content of lump ceramic phases is few. According to Fig. 9(c) and (d), one can find many ceramic particles uniform distribution in the wear surface. Under the help of the multi-ring phase (Ti, Nb, Mo) (C, N) and MCx, the coatings of these specimen (specimens 3# and 4#) show a low friction coefficient, which is a factor 3.98 and 4.44 times smaller than that of pure Ni204-based alloy coating. According to Fig. 9(a1)-(e1), all specimens revealed a flatter wear surface. Compared with the literature [19], the in situ synthesis ceramic particles have effectively reduced surface wear of

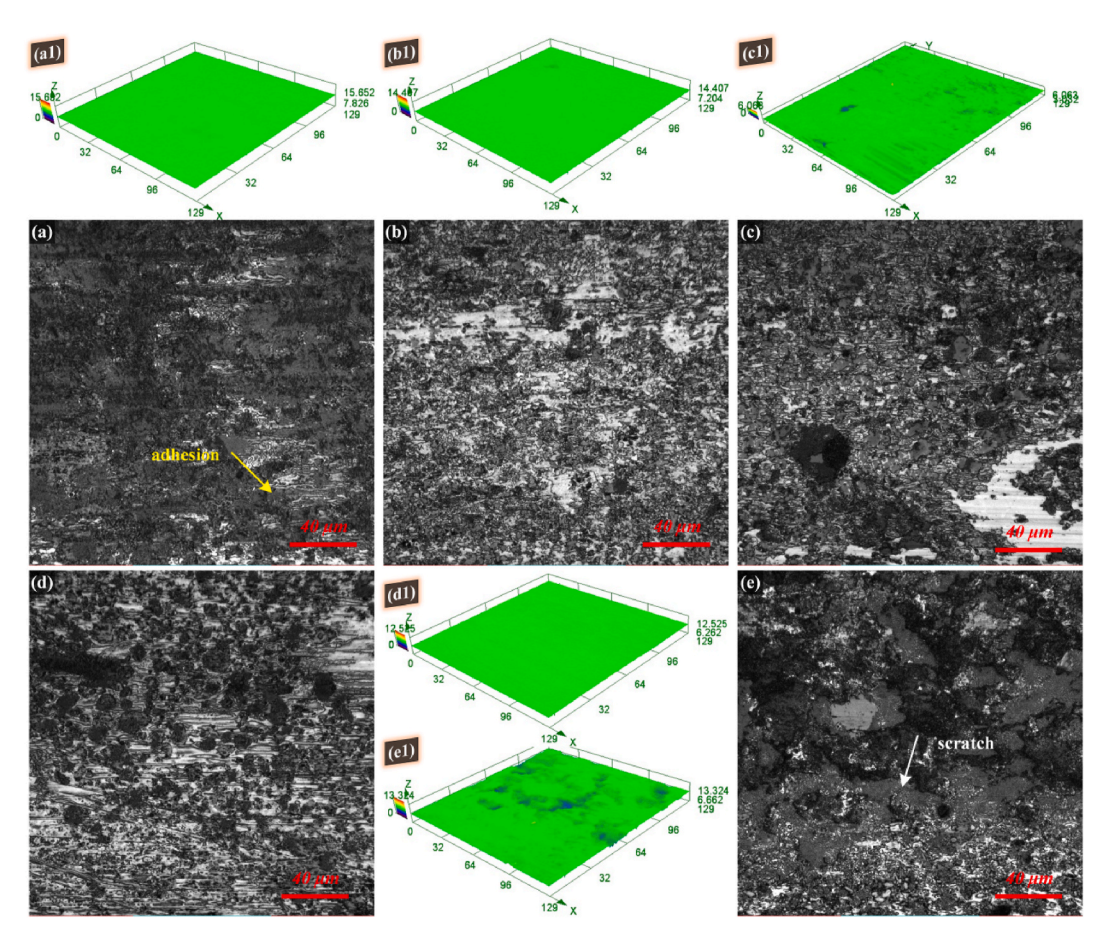


Fig. 9. Wear morphologies of different samples.

Ni204-based alloy coating.

#### 4. Conclusions

In this study, TiC-, TiN- and Ti(C, N)-reinforced Ni204 alloy coatings were in situ formed via laser cladding. The enhancement of Ti–C–TiN–Ni204 on the microstructure, microhardness, and tribomechanical properties was investigated. Besides, the element diffusion and microstructure characteristics in the interface between the coating and substrate were also studied.

- (1) TiC, TiN, Ti(C, N), multi-phase or ring phase (Ti, Mo, Nb) (C, N), and MC<sub>x</sub> (M = Fe, Cr, Nb, and Mo) were in situ synthesized in the composite coating. The addition of C particles promoted the generation of multi-phase, ring phase, and carbides, thus improving the bonding strength between the reinforcement phase and the matrix.
- (2) The reinforcement phases were most uniformly distributed in the composite coating that was added Ti, C, and TiN particles to the coating at the same time. The (Ti, Nb, and Mo), ceramic phase, and carbides partially replace (Nb, Mo) phase at the grain boundary. Meanwhile, in situ synthesis tiny TiC particles dissolved into the matrix to reinforce the hardness and wear of the coating. Furthermore, the diffusion activities have become established in the interface between substrate and coating.
- (3) The ring phase (Ti, Mo, Nb) (C, N), Ti(C, N), and MC<sub>x</sub> improved the deformation resisting capability. The coatings with 5:1 mass fraction ratio of TiN/C (specimen 5#) and 21:7:2 mass fraction ratio of TiN/Ti/C (specimen 4#) exhibited the highest microhardness and lowest friction coefficient, respectively. The microhardness of specimen 5 is 1127.3 HV<sub>0.5</sub>, which is 3.78 times higher than that of the original Ni204 coating. The friction coefficient of specimen 4# is 4.44 times smaller than that of the original Ni204 coating.
- (4) The microhardness and tribo-mechanical properties are synthetically determined by the content, size, kind, and characteristic of the reinforcement phases. The formation of Ti- and *C*-rich phases can effectively relieve the floating up of the tiny ceramic particles and improve the microhardness at the bottom of the coating.

#### Declaration of competing interest

We declare that we have no financial and personal relationships with other peoples or organizations that can inappropriately influence our work. There is no professional or other personal interest of any nature or kind in any product, service and/or company that could be construed as influencing the position presented in, or the review of. The manuscript entitled, "Microstructure and mechanical properties of Ti–C–TiN-reinforced Ni204-based laser-cladding composite coating".

# Acknowledgments

This work was support by the Fundamental Research Funds for the Central Universities (N180306004, N2003026); the Ministry of Industry and Information Technology of China under Grant (No. 201675514); the Science and Technology Planning Project of Shenyang under Grant (No.18006001).

#### References

- Y. Chen, W. Gong, R. Kang, Review and propositions for the sliding/impact wear behavior in a contact interface, Chin. J. Aeronaut. 33 (2020) 391–406, https://doi. org/10.1016/j.cja.2018.06.004.
- [2] Q. Ji, C. Li, D. Zhu, Y. Jin, Y. Lv, J. He, Structural design optimization of moving component in CNC machine tool for energy saving, J. Clean. Prod. 246 (2020) 118976, https://doi.org/10.1016/j.jclepro.2019.118976.

- [3] W. Kusdiana, A. Nugroho, A. Rahman, Analysis of fuel quality effect on the life time from high-pressure pump of engine mtu 12 V 4000 M 71, Int. J. ASRO. 11 (2020) 193–200
- [4] Y. Wang, Z. Jiang, X. Hu, C. Li, Optimization of reconditioning scheme for remanufacturing of used parts based on failure characteristics, Robot. Comput. Integrated Manuf. 61 (2020), https://doi.org/10.1016/j.rcim.2019.101833.
- [5] T. Hussain, D.G. McCartney, P.H. Shipway, D. Zhang, Bonding mechanisms in cold spraying: the contributions of metallurgical and mechanical components, J. Therm. Spray Technol. 18 (2009) 364–379, https://doi.org/10.1007/s11666-009-9298-1.
- [6] M. Liang, W. Wan, Z. Guo, J. Xiong, G. Dong, X. Zheng, Y. Chen, P. Liu, Erosion-corrosion behavior of Ti(C,N)-based cermets with different TiN contents, Int. J. Refract. Metals Hard Mater. 43 (2014) 322–328, https://doi.org/10.1016/j.iimphm.2013.10.006.
- [7] X. Wang, Z. Zhang, Y. Men, X. Li, Y. Liang, L. Ren, Fabrication of nano-TiC functional gradient wear-resistant composite coating on 40Cr gear steel using laser cladding under starved lubrication conditions, Optic Laser. Technol. 126 (2020) 106136, https://doi.org/10.1016/j.optlastec.2020.106136.
- [8] L. Yang, T. Yu, M. Li, Y. Zhao, J. Sun, Microstructure and wear resistance of in-situ synthesized Ti(C, N) ceramic reinforced Fe-based coating by laser cladding, Ceram. Int. 44 (2018) 22538–22548, https://doi.org/10.1016/j.ceramint.2018.09.025.
- [9] J.I. Arrizubieta, O. Ukar, M. Ostolaza, A. Mugica, Study of the environmental implications of using metal powder in additive manufacturing and its handling, Metals 10 (2020), https://doi.org/10.3390/met10020261.
- [10] M. Zhang, H. Yao, H. Wang, Q. Chen, X. Bai, X. Zhao, Y. Fang, H. Xu, Q. Li, In situ Ti(C,N)-based cermets by reactive hot pressing: reaction process, densification behavior and mechanical properties, Ceram. Int. 45 (2019) 1363–1369, https:// doi.org/10.1016/j.ceramint.2018.07.270.
- [11] L.A. Dobrzański, M. Adamiak, Structure and properties of the TiN and Ti(C,N) coatings deposited in the PVD process on high-speed steels, J. Mater. Process. Technol. 133 (2003) 50–62, https://doi.org/10.1016/S0924-0136(02)00244-3.
- [12] Y. You, A. Ito, R. Tu, T. Goto, Laser chemical vapor deposition of TiN film on Ti(C, N)-based cermet substrate using Ti(OiPr)2(dpm)2-NH3 system, J. Ceram. Soc. Japan. 119 (2011) 310–313, https://doi.org/10.2109/jcersj2.119.310.
- [13] P.V. Badiger, V. Desai, M.R. Ramesh, Development and characterization of Ti/TiC/ TiN coatings by cathodic arc evaporation technique, Trans. Indian Inst. Met. 70 (2017) 2459–2464, https://doi.org/10.1007/s12666-017-1107-9.
- [14] Q. Yang, W. Xiong, M. Zhang, B. Huang, S. Chen, Microstructure and mechanical properties of Mo-free Ti(C,N)-based cermets with Ni-xCr binders, J. Alloys Compd. 636 (2015) 270–274, https://doi.org/10.1016/j.jallcom.2014.11.236.
- [15] E. Shankar, S.B. Prabu, Microstructure and mechanical properties of Ti (C, N) based cermets reinforced with different ceramic particles processed by spark plasma sintering, Ceram. Int. 43 (2017) 10817–10823, https://doi.org/10.1016/j. ceramint.2017.05.103.
- [16] Y. Zhao, T. Yu, J. Sun, W. Xi, X. Bi, Effect of laser cladding on forming qualities of YCF101 alloy powder in the different lap joint modes, Int. J. Adv. Manuf. Technol. 96 (2018) 1991–2001. https://doi.org/10.1007/s00170-018-1732-4.
- [17] Y. Zhao, T. Yu, Z. Wang, H. Chen, Calculation and verification of Start/Stop optimum overlapping rate on metal DLF technology, Int. J. Adv. Manuf. Technol. 99 (2018) 437–452. https://doi.org/10.1007/s00170-018-2445-4.
- 99 (2018) 437–452, https://doi.org/10.1007/s00170-018-2445-4.
  [18] T. Yu, Y. Zhao, J. Sun, Y. Chen, W. Qu, Process parameters optimization and mechanical properties of forming parts by direct laser fabrication of YCF101 alloy, J. Mater. Process. Technol. 262 (2018) 75–84, https://doi.org/10.1016/j.imatprotec. 2018.06.023
- [19] Y. Zhao, T. Yu, C. Guan, J. Sun, X. Tan, Microstructure and friction coefficient of ceramic (TiC, TiN and B4C) reinforced Ni-based coating by laser cladding, Ceram. Int. 45 (2019) 20824–20836, https://doi.org/10.1016/j.ceramint.2019.07.070.
- [20] I. Saravanan, A. Elaya Perumal, S.C. Vettivel, N. Selvakumar, A. Baradeswaran, Optimizing wear behavior of TiN coated SS 316L against Ti alloy using Response Surface Methodology, Mater. Des. 67 (2015) 469–482, https://doi.org/10.1016/j. matdes 2014 10 051
- [21] T. Chen, F. Wu, H. Wang, D. Liu, Laser cladding in-situ Ti(C,N) particles reinforced ni-based composite coatings modified with CeO2 nanoparticles, Metals 8 (2018), https://doi.org/10.3390/met8080601.
- [22] Y. Zhao, T. Yu, J. Sun, S. Jiang, Microstructure and properties of laser cladded B4C/TiC/Ni-based composite coating, Int. J. Refract. Metals Hard Mater. 86 (2020) 105112, https://doi.org/10.1016/j.ijrmhm.2019.105112.
- [23] Department of Inorganic Chemistry, Dalian University of Technology, Inorganic Chemistry, Higher Education Press, vol. 5 (2006) 675-689.
- [24] L. Yang, T. Yu, M. Li, Y. Zhao, J. Sun, Microstructure and wear resistance of in-situ synthesized Ti(C, N) ceramic reinforced Fe-based coating by laser cladding, Ceram. Int. 44 (2018) 22538–22548, https://doi.org/10.1016/j.ceramint.2018.09.025.
- [25] M. Wang, H. Cui, N. Wei, L. Ding, X. Zhang, Y. Zhao, C. Wang, Q. Song, A new design of in situ Ti(C,N) reinforced composite coatings and their microstructures, interfaces, and wear resistances, ACS Appl. Mater. Interfaces 10 (2018) 4250–4265, https://doi.org/10.1021/acsami.7b17286.
- [26] Y. Zhao, Y. Zheng, W. Zhou, J. Zhang, G. Zhang, W. Xiong, Microstructure and performance of functionally gradient Ti(C, N)-based cermets fabricated by lowpressure carburizing treatment during liquid phase sintering, Ceram. Int. 43 (2017) 1956–1962, https://doi.org/10.1016/j.ceramint.2016.10.159.
- [27] J.H. Jang, Y.U. Heo, C.H. Lee, H.K.D.H. Bhadeshia, D.W. Suh, Interphase precipitation in Ti-Nb and Ti-Nb-Mo bearing steel, Mater. Sci. Technol. 29 (2013) 309–313, https://doi.org/10.1179/1743284712Y.0000000131.
- [28] R. Sun, W. Lu, X. Yang, Microscopic morphology and distribution of TiC phase in laser clad TiC-NiCrBSi cermet layer, Kuei Suan Jen Hsueh Pao/J. Chinese Ceram. Soc. 33 (2005) 1448–1452.

- [29] M. Azadi, A.S. Rouhaghdam, S. Ahangarani, Mechanical behavior of TiN/TiC-n multilayer coatings and Ti(C,N) multicomponent coatings produced by PACVD,
  Strength Mater. 48 (2016) 279–289, https://doi.org/10.1007/s11223-016-9763-2.
  [30] Z.P. Tong, X.D. Ren, W.F. Zhou, S. Adu-Gyamfi, L. Chen, Y.X. Ye, Y.P. Ren, F.Z. Dai,
- J.D. Yang, L. Li, Effect of laser shock peening on wear behaviors of TC11 alloy at
- elevated temperature, Optic Laser. Technol. 109 (2019) 139-148, https://doi.org/ 10.1016/j.optlastec.2018.07.070
- [31] X. Ren, Z. Tong, W. Zhou, L. Chen, Y. Ren, F. Dai, Y. Ye, S. Adu-Gyamfi, J. Yang, L. Li, High temperature wear performance of Ti-6.5Al-3.5Mo-1.5Zr-0.3Si alloy subjected to laser shock peening, Mater. Sci. Technol. 34 (2018) 2294–2304, https://doi.org/10.1080/02670836.2018.1530490.